

**Zeitschrift:** Helvetica Physica Acta  
**Band:** 51 (1978)  
**Heft:** 2  
  
**Artikel:** X-ray study of the low temperature phases of alkali hyperoxides  
**Autor:** Rosenfeld, M. / Ziegler, M. / Känzig, W.  
**DOI:** <https://doi.org/10.5169/seals-114949>

### **Nutzungsbedingungen**

Die ETH-Bibliothek ist die Anbieterin der digitalisierten Zeitschriften auf E-Periodica. Sie besitzt keine Urheberrechte an den Zeitschriften und ist nicht verantwortlich für deren Inhalte. Die Rechte liegen in der Regel bei den Herausgebern beziehungsweise den externen Rechteinhabern. Das Veröffentlichen von Bildern in Print- und Online-Publikationen sowie auf Social Media-Kanälen oder Webseiten ist nur mit vorheriger Genehmigung der Rechteinhaber erlaubt. [Mehr erfahren](#)

### **Conditions d'utilisation**

L'ETH Library est le fournisseur des revues numérisées. Elle ne détient aucun droit d'auteur sur les revues et n'est pas responsable de leur contenu. En règle générale, les droits sont détenus par les éditeurs ou les détenteurs de droits externes. La reproduction d'images dans des publications imprimées ou en ligne ainsi que sur des canaux de médias sociaux ou des sites web n'est autorisée qu'avec l'accord préalable des détenteurs des droits. [En savoir plus](#)

### **Terms of use**

The ETH Library is the provider of the digitised journals. It does not own any copyrights to the journals and is not responsible for their content. The rights usually lie with the publishers or the external rights holders. Publishing images in print and online publications, as well as on social media channels or websites, is only permitted with the prior consent of the rights holders. [Find out more](#)

**Download PDF:** 07.08.2025

**ETH-Bibliothek Zürich, E-Periodica, <https://www.e-periodica.ch>**

# X-ray study of the low temperature phases of alkali hyperoxides

by M. Rosenfeld<sup>1)</sup>, M. Ziegler<sup>2)</sup> and W. Känzig

Laboratory of Solid State Physics, Swiss Federal Institute of Technology, 8093 Zürich, Switzerland

(18.I.1978)

*Abstract.* By means of X-ray single crystal diffraction the different phases of  $\text{KO}_2$ ,  $\text{RbO}_2$  and  $\text{CsO}_2$  were studied in the temperature range 5–200 K. The formation of crystallographic domains, the symmetry and the dimensions of the unit cell in the different phases were investigated. Phase V ( $7 \text{ K} < T < 12 \text{ K}$ ) of  $\text{KO}_2$  is a mixture of the triclinic structure of phase VI ( $T < 7 \text{ K}$ ) and the monoclinic structure of phase IV ( $12 \text{ K} < T < 196 \text{ K}$ ). In  $\text{RbO}_2$  and  $\text{CsO}_2$ , the modulated structure of phase III persists upon cooling into the lower temperature phases down to 5 K. Phase III of  $\text{RbO}_2$  can be divided into 3 subphases with different symmetries. At the transition III/(IV)/V no change in symmetry has been observed. In  $\text{CsO}_2$  the whole phase III and phase IV have the same symmetry.

## 1. Introduction

The alkali hyperoxides  $\text{NaO}_2$ ,  $\text{KO}_2$ ,  $\text{RbO}_2$  and  $\text{CsO}_2$  are interesting compounds because they undergo a sequence of phase transitions involving orientational order of the paramagnetic anion  $\text{O}_2^-$ , and in some cases possibly magnetic order at low temperatures. The magnetic and caloric properties are known [1]. The structures of the phases above liquid nitrogen temperature are relatively well investigated [2]. Neutron diffraction data of  $\text{NaO}_2$  [2, 3] and  $\text{KO}_2$  [4] are incomplete. Antiferromagnetic order has been detected in  $\text{KO}_2$  below 7 K. For a review of recent work see reference [5].

The present work is an extension to low temperatures of the X-ray investigations of  $\text{KO}_2$ ,  $\text{RbO}_2$  and  $\text{CsO}_2$  described in reference [2] and has to be read in conjunction with it. One aim was to correlate the crystallographic with the magnetic properties in view of a possible interdependence of molecular and magnetic order.

The symmetries of the low temperature phases are so low that a successful analysis of the Debye–Scherrer patterns is impossible. Therefore single crystals were used in the present work. It turned out that the sequence of phase transitions gives rise to complicated arrays of crystallographic domains. The analysis of the X-ray patterns yielded the deformations of the unit cell that occur at the phase transitions. For  $\text{KO}_2$  the deformation present in the phases where magnetic order begins is surprisingly large.

The nomenclature of the phases is taken from the work on magnetic and caloric properties [1].

<sup>1)</sup> Present address: Mettler Optic AG, CH-8606 Greifensee.

<sup>2)</sup> Present address: Kantonsschule Limmattal, CH-8902 Urdorf.

## 2. Experimental

Small single crystals of  $\text{KO}_2$ ,  $\text{RbO}_2$  and  $\text{CsO}_2$  were grown in liquid ammonia (temperature range of phase II) by a technique described elsewhere [6, 7]. For the X-ray experiments the very hygroscopic crystals were sealed in Lindemann-glass tubes in an atmosphere of dry helium gas. They were oriented on a Buerger-precession goniometer and transferred (together with the goniometer head) to a low temperature Weissenberg camera. A continuous flow He-cryostat of the type described by Klipping [8, 9, 10] was made small enough to fit into a suitably modified commercial 57.3 mm Weissenberg camera [11]. The Lindemann capillary is immersed in the gas stream. The cryostat worked so well that it will be described here.

The rotating shaft of the commercial camera was replaced by a superinsulated helium transfer tube, on the end of which can be mounted a small goniometer head [12]. The transfer tube is connected to a 100 liter liquid helium vessel through a rotating joint outside the camera. A cross-section through the cryostat is given in Figure 1. The third or upper base of the camera (Buerger's designation [13]) had to be extended by a spacer in order to accommodate a sufficiently long thermal conduction path. Figure 2 shows the assembly and the modification of the commercial camera. The temperature is stabilized as described in [10]. The stability below 15 K is limited to about  $\pm 0.5$  K (over a period of up to one week) by helium oscillations in the horizontal cryostat. The consumption of liquid helium as a function of sample

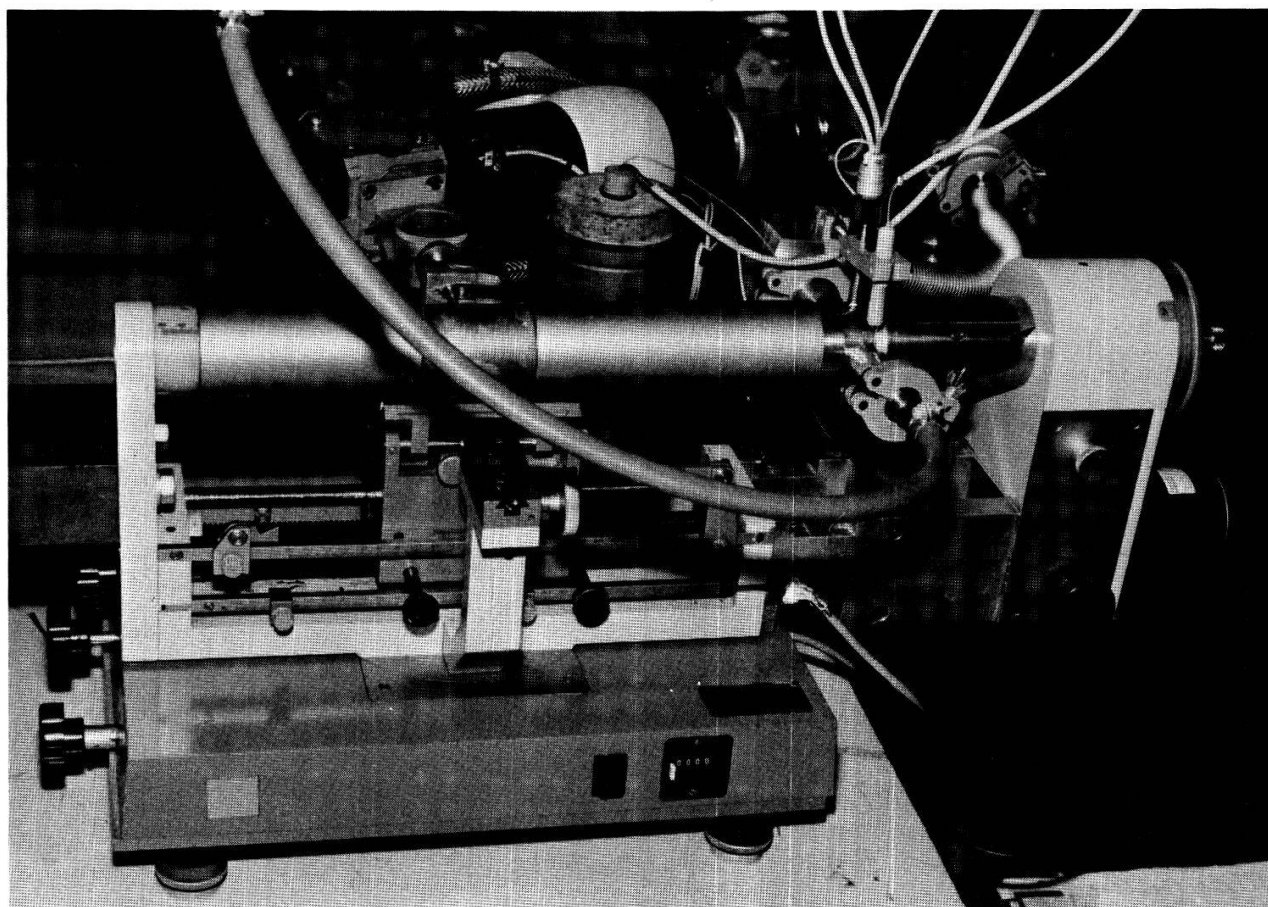


Figure 2  
The Weissenberg goniometer with assembled cryostat (film cylinder removed).

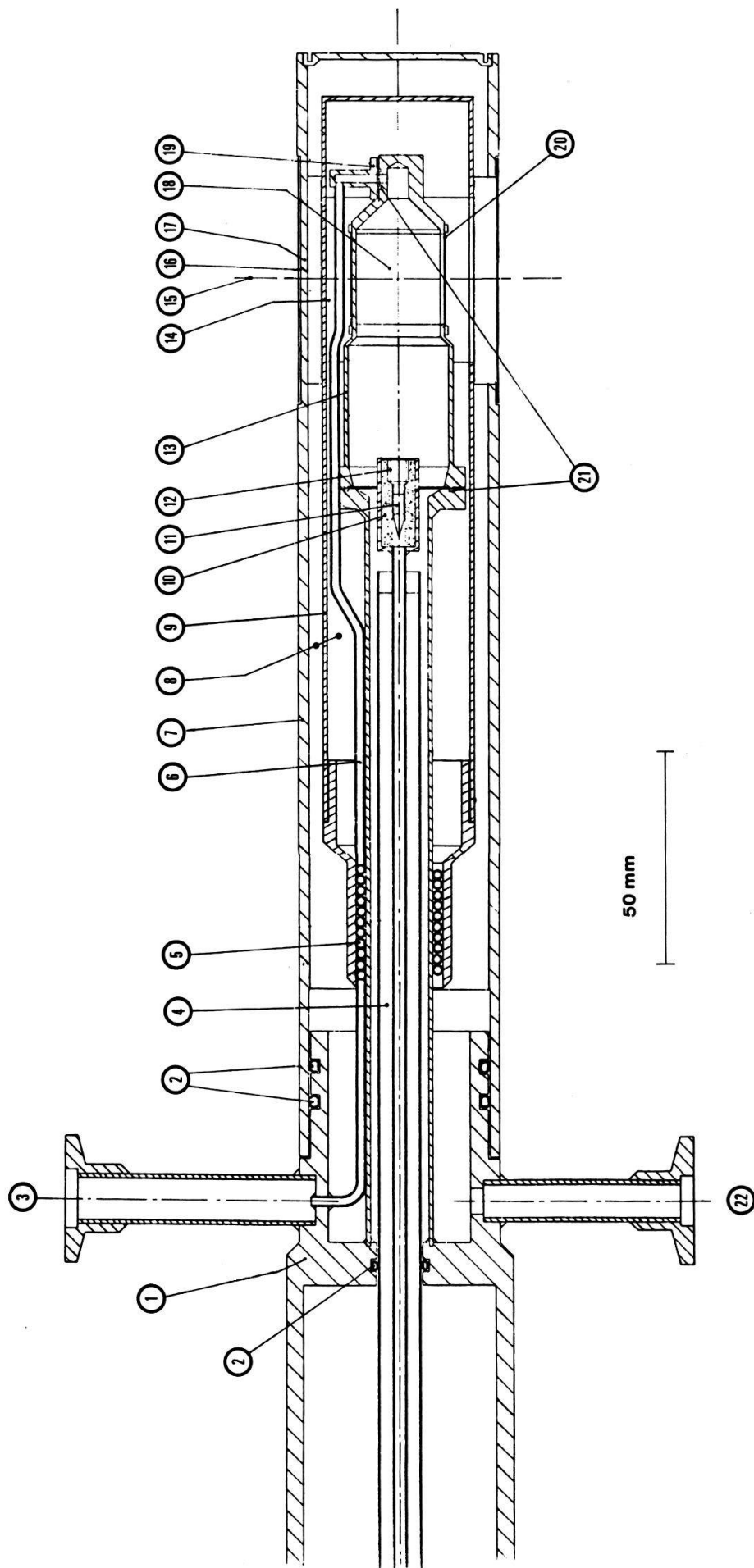


Figure 1

A cross-section through the X-ray cryostat. Screens preventing unwanted scattering from the entrance window and electrical connections are not shown:

- |    |  |    |   |
|----|--|----|---|
| 1  | Support of the cryostat, rigidly connected to the X-ray camera | 12 | thread for goniometer head                        |
| 2  | O-rings  | 13 | stainless steel cylinder with beryllium window 20 |
| 3  | helium exhaust to pumping system                               | 14 | aluminized mylar window                           |
| 4  | helium transfer tube (coaxial to camera)                       | 15 | axis of X-ray beam                                |
| 5  | heat exchanger for cooling of radiation shield 9               | 16 | beryllium window of vacuum cylinder, 0.5 mm thick |
| 6  | helium return  | 17 | connecting bridge                                 |
| 7  | stainless steel vacuum cylinder with beryllium window 16       | 18 | sample chamber                                    |
| 8  | isolation vacuum (communicating)                               | 19 | flange of the helium return tube                  |
| 9  | copper radiation shield with aluminized mylar window 14        | 20 | beryllium window of sample chamber, 0.1 mm thick  |
| 10 | porous sintered metal cylinder                                 | 21 | indium seals                                      |
| 11 | adjustable needle valve  | 22 | to high vacuum system.                            |



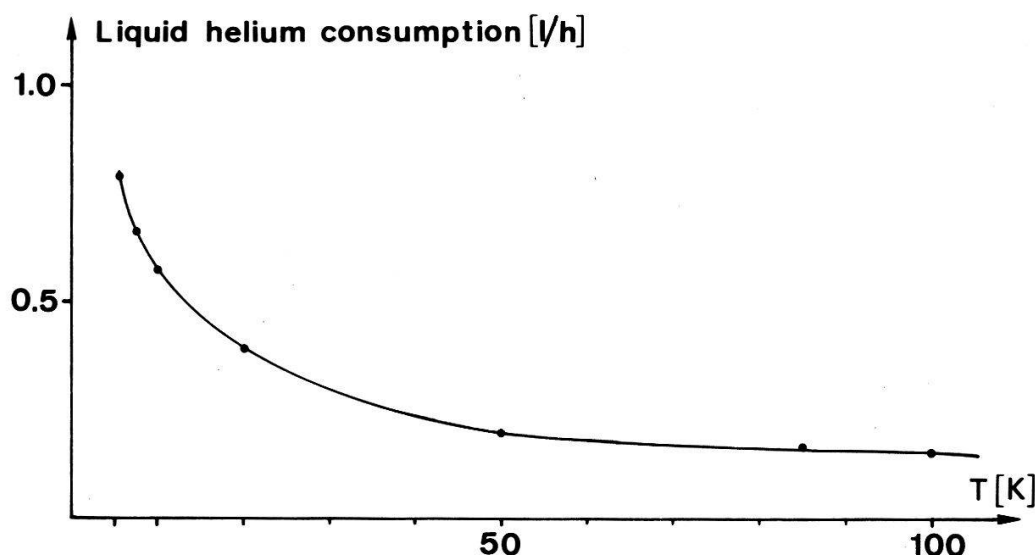


Figure 3  
Liquid helium consumption as function of the sample temperature.

temperature is given in Figure 3. The temperature is measured by a Au(0.07 at % Fe)/chromel thermocouple and a carbon resistor located in the gas stream at a distance of about 2 mm from the crystal.

### 3. $\text{KO}_2$

The structures of the low temperature phases known from previous and the present work are summarized in Figure 4. In phase II the orthorhombic distortion of the lattice is so small that the splitting of the reflections due to domain formation cannot be resolved. However, the orthorhombic symmetry can be inferred from the intensities [2]. In the following we use the pseudotetragonal  $bc$  cell of phase II ( $I 4/\text{mm}$ ) as reference system in all low temperature phases if not stated otherwise.

#### 3.1. Polarization microscopy of phase III ( $196 \text{ K} < T < 231 \text{ K}$ )

A study of the ferroelastic domains was possible on thin crystal platelets ( $5 \times 5 \times 0.1 \text{ mm}^3$ ) that were grown in liquid ammonia containing  $[(\text{CH}_3)_4\text{N}]\text{O}_2$  [6, 7]. At the II  $\rightarrow$  III phase transition temperature (231 K), spear-like domains parallel to  $[110]$  and  $[1\bar{1}0]$  appear (see Figure 5). The domain walls appear as thin dark lines. The domains grow with decreasing temperature, their mean width is about 0.02 mm at 210 K. During the phase transition III  $\rightarrow$  IV at 196 K one observes a transient increase of sample transparency. Lowering the temperature further the sample becomes opaque.

#### 3.2. Phase IV ( $12 \text{ K} < T < 196 \text{ K}$ )

In crystals cooled from phase II through phase III into phase IV, four domain orientations are inferred from the splitting of the reflections. The twin angle designated by  $\psi$  in reference [19] increases from  $4.2^\circ$  at 170 K [19] to  $6.9^\circ$  at 55 K. Presumably this change is related to an increase of the tilt angle  $\phi$  of the molecule axis

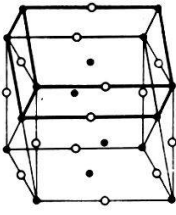
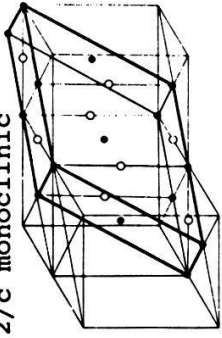
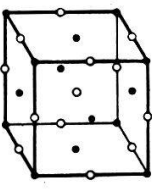
| KO <sub>2</sub>              |  |   |  |       |
|------------------------------|--|---|--|-------|
| Phase transition temp.       | Symmetry and choice of unit cell<br>O Anion O <sub>2</sub> <sup>2-</sup> / • Kation K <sup>+</sup>                     | State of order  | Lattice constant<br>Volume of unit cell  |       |
| II<br>[2,14,15,<br>16,17,18] | orthorhombic (pseudotetragonal)<br> | Stacking of planes differing in molecular orientation and displacement. Diffraction satellites very diffuse.<br>(paramagnetic)    | a = b = 4.033 ± 0.002 Å<br>c = 6.699 ± 0.002 Å<br>V <sub>II</sub> = 108.960 Å <sup>3</sup>   | 293 K |
| — 231 K                      |  |   |  |       |
| III<br>[2,*]                 |  | incommensurate superstructure (as RbO <sub>2</sub> III, CsO <sub>2</sub> III)   |  |       |
| — 196 K                      |  |   |  |       |
| IV<br>[2,19,*]               | C 2/c monoclinic<br>                | Molecular order:<br>molecules in a domain are parallel.<br>Commensurate superstructure referred to bc-cell, 2a.<br>(paramagnetic) | a = 7.880 ± 0.005 Å<br>b = 4.036 ± 0.005 Å<br>c = 7.968 ± 0.005 Å<br>β = 122.85 ± 0.05 °<br>V <sub>IV</sub> = 212.890 Å <sup>3</sup> = 1,954 V <sub>II</sub>                           | 140 K |
| 12.1 K ↑<br>10.6 K ↑         |  |   |  |       |
| V<br>[20,*]                  | coexistence of X-ray crystallographic structures of phases IV and VI<br>(magnetic order unknown)                       |   |  |       |
| — 7.1 K                      |  |   |  |       |
| VI<br>[4,*]                  | F $\bar{1}$ triclinic<br>         | Molecular order:<br>molecules in a domain are parallel.<br>(antiferromagnetic)  | a = 5.96 ± 0.01 Å<br>b = 5.43 ± 0.01 Å<br>c = 6.59 ± 0.01 Å<br>α = 94.0 ± 0.1 °<br>β = 87.5 ± 0.1 °<br>γ = 90.00 °<br>V <sub>VI</sub> = 212.548 Å <sup>3</sup> = 0.998 V <sub>IV</sub> | 7,5 K |

Figure 4

Survey over the structures of the low temperature phases of KO<sub>2</sub>. \* means reference to the present work. ↓ and ↑ designate decreasing and increasing temperature, respectively.

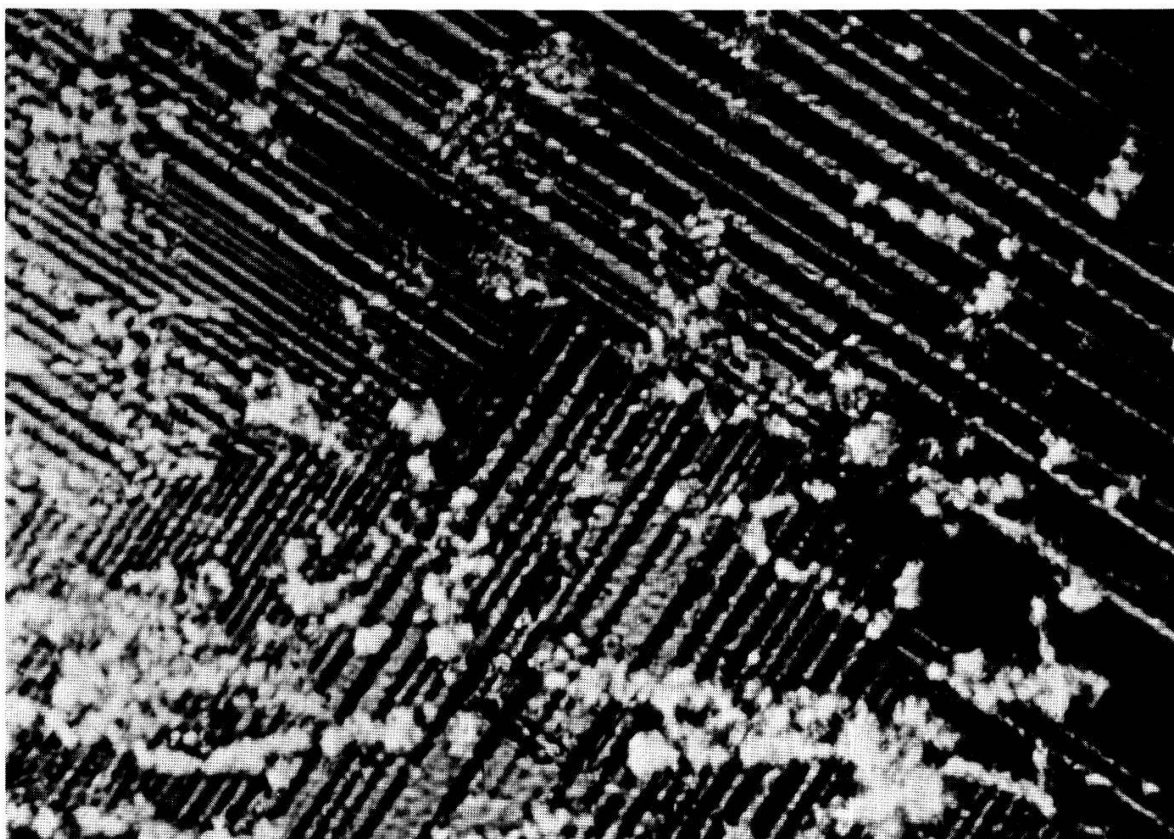


Figure 5

Photograph of  $\text{KO}_2$  in phase III with polarized light (crossed nicols),  $[001]$  perpendicular to the plane of the paper.

with respect to  $[001]$ . X-ray diffraction at 170 K yielded  $10^\circ < \phi < 20^\circ$  [19], whereas paramagnetic resonance at 13 K gave  $\phi = 21^\circ$  [20].

### 3.3. Phases V ( $7.1 \text{ K} < T < 12 \text{ K}$ ) and VI ( $T < 7.1 \text{ K}$ )

The main obstacle in the structure determination of the low temperature phases is the domain structure. The crystals were oriented and mounted in the cryostat at room temperature (phase II). On cooling the crystals through the phases III, IV and V into phase VI, twinning occurs at each transition with the exception  $V \rightarrow VI$ . The twinning angles in the phases V and VI are so large that in rotating crystal photographs different layer lines from different domains intersect (see Figure 7 (a)).

**3.3.1. Sample mounting.** Referring to the  $bc$  cell of phase II the rotation axis was chosen parallel to

- (1)  $[100]$
- or (2)  $[110]$
- or (3)  $[001]$ .

The shape of the crystals was usually a rectangular parallelepiped. A typical size was  $0.3 \times 0.3 \times 0.2 \text{ mm}^3$  with the shortest edge parallel to  $[001]$  and the other two edges parallel and perpendicular to  $[110]$ . The crystals were put into the Lindemann-glass capillary with the  $[110]$ -axis parallel to the tube axis. For orientation (2) the

capillary was mounted parallel to the rotation axis and for orientation (1) with a  $45^\circ$  tilt. For orientation (3) the crystals were put into the capillary with the  $[001]$ -axis parallel to the tube axis.

### 3.3.2. Twinning pattern and cell dimensions.

*Coexistence of the structures of phases IV and VI in the temperature range of phase V.* Rotating crystal and Weissenberg equi-inclination photographs of crystals in orientation (1) of phases IV and V are shown in Figures 6 and 7, respectively. At the

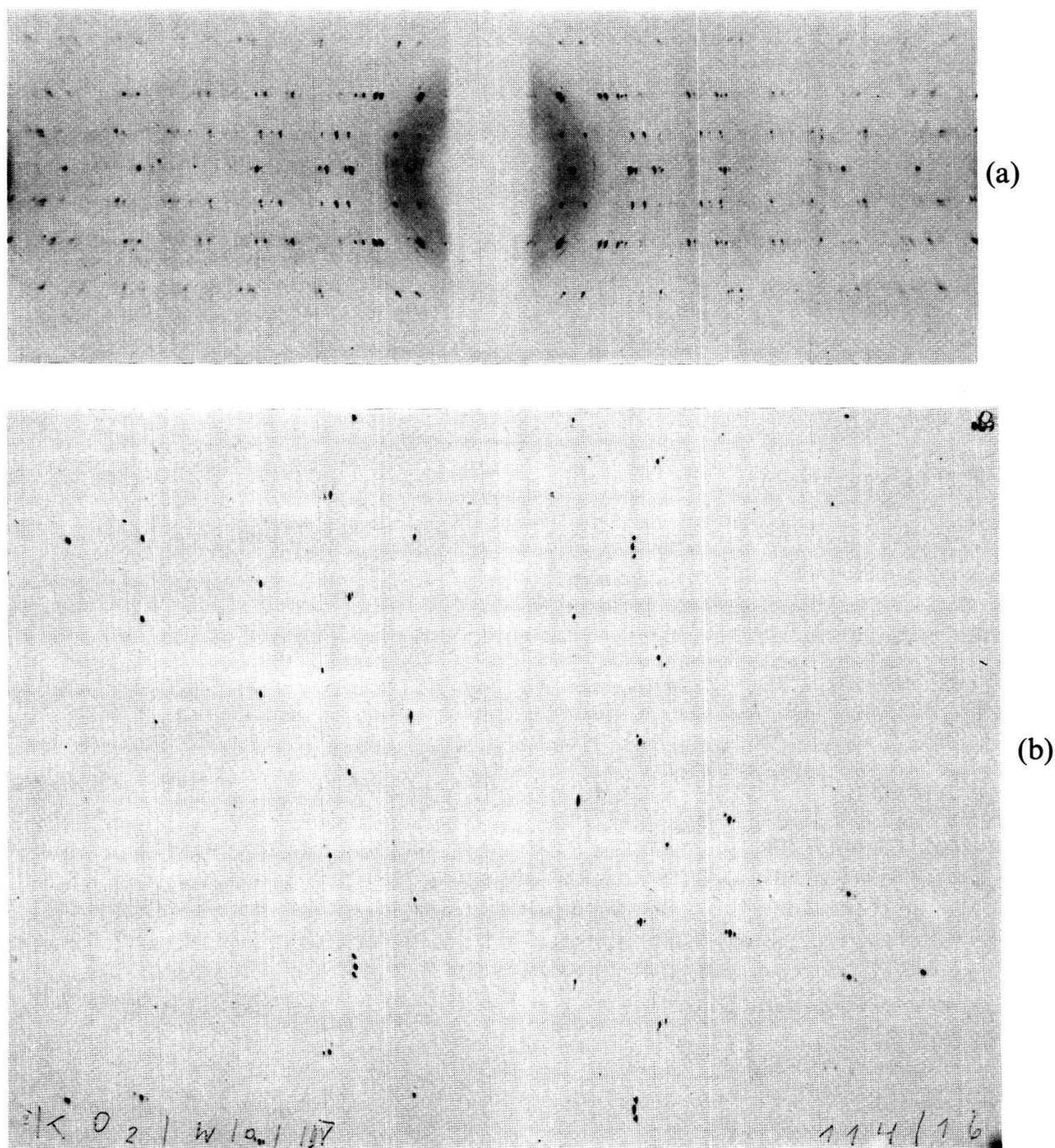


Figure 6  
X-ray diffraction of  $\text{KO}_2$  phase IV, 120 K, crystal rotated about  $[100]$  (referred to the  $bc$  cell of phase II),  $\text{CuK}_\alpha$ -radiation (graphite monochromator): (a) rotating crystal photograph, (b) Weissenberg zero level photograph.



transition from phase IV into phase V all reflections of phase IV with the exception of  $00l$  split into groups of several reflections. Upon closer inspection it was noted that every original reflection of phase IV was also present in phase V. However, new reflections *between* the groups have not been observed. One concludes that neither a superstructure nor new symmetry elements appear.

In phase V the reflections of a group can be divided into two classes, each corresponding to a distinct structure. The first class consists of *weak* reflections that

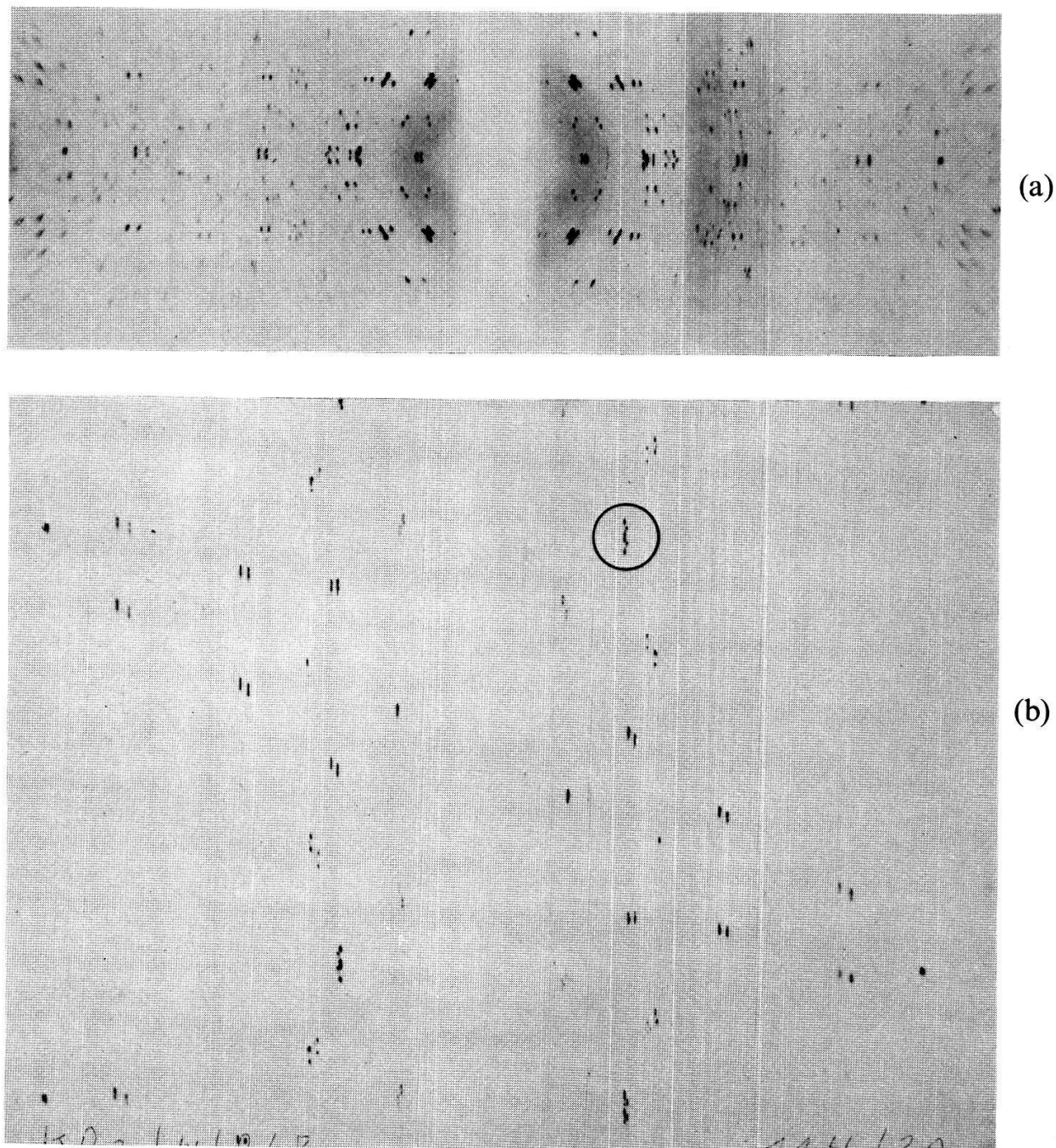


Figure 7

X-ray diffraction of  $\text{KO}_2$  phase V, 7.5 K, crystal rotated about  $[100]$  (referred to the  $bc$  cell of phase II),  $\text{CuK}_\alpha$ -radiation (graphite monochromator).

(a) Rotating crystal photograph.

(b) Weissenberg zero level photograph. The two less intense spots in the marked circle belong to the structure of phase IV and can be recognized in Figure 6 (b).

stay at exactly the same position as the original reflections of phase IV throughout the transition IV  $\rightarrow$  V. These reflections become weaker with decreasing temperature and disappear if the Néel point at 7 K is approached. The second class consists of *strong* reflections that stay unchanged in position over the transition V  $\rightarrow$  VI at 7 K. Thus, in the temperature range 7–12 K corresponding to phase V, one observes coexistence of the X-ray diffraction patterns of phases IV and VI. The space group of phase VI is a subgroup of the space group C 2/c of phase IV. Unfortunately the intensities of the split reflections cannot be measured with sufficient accuracy to permit a determination of the atomic parameters.

The following arguments indicate that this coexistence is not an artifact due to experimental shortcomings such as insufficient temperature stability of the cryostat and inhomogeneous temperature distribution in the sample:

- (1) The temperature stability of the cryostat is about  $\pm 0.5$  K whereas the weak reflections persist over a temperature range of 3.5 K on cooling. The thermal hysteresis of the transition IV/V derived from magnetic measurements is 1.5 K [1].
- (2) Temperature gradients in the crystal due to volume heating by the X-ray beam and cooling through the surface can be excluded since a reduction of the X-ray intensity by a factor of about ten did not change the intensity ratio between the weak and the strong reflections.

*The number of different twin domain orientations (henceforth called domains).* In order to discuss the number of domains in phase VI we must consider first the four domain orientations in phase IV mentioned in Section 3.2. In this phase the superstructure (referred to phase II) is strictly commensurate (doubling) [2, 19]. The twinning pattern is such that the superlattice reflections arising from different domains appear at entirely different positions in reciprocal space. In phase VI every one of these reflections splits into two reflections. This means that each domain of phase IV produces two different domain orientations in phase VI. Thus phase VI has 8 different domain orientations.

At the transition from a high temperature (parent) structure of space group G to a low temperature (derived) structure of space group F, one or more symmetry elements are lost. Group theory predicts the number of possible domain orientations that may arise from a given parent domain at the phase transition [21–25]. The number of domains is given by  $n_G/n_F$ , where  $n_G$  and  $n_F$  are the orders of the point groups of G and F, respectively.

The space group C 2/c of phase IV has the point symmetry  $2/m$  with the subgroups 2,  $m$  and  $\bar{1}$  (we cannot distinguish between  $\bar{1}$  and 1 in the diffraction pattern because of Friedel's law). Thus  $G = C 2/c$  and  $n_G = 4$ . For all possible subgroups one has  $n_F = 2$  and therefore the number of possible domains of the derived structure is 2 for every one of the four domains in phase IV. This is in accordance with the observed number of domains.

At the transition IV/V the magnetic susceptibility makes a discontinuous jump [1]. The transition is of the first order. This manifests itself also in the following fact. The reflections belonging to the diffraction pattern of the structures of phases IV and VI have upon cooling at 10 K (only 0.6 K below the transition IV  $\rightarrow$  V) about the same intensity. One concludes that about two-thirds of the crystal volume (volume



fraction of domains of phase VI divided by the volume fraction of domains in phase IV) has already the crystallographic structure of phase VI.

*Indexing the reflections – unit cell dimensions.* In order to determine the dimensions of the unit cell, one has to identify the reflections belonging to each domain. As a guide one can use a model of the twinning that originates from group theory [21–25]. Twin domains transform into each other by a point symmetry operation which is lost at the phase transition. (Antiphase domains giving rise to satellite reflections are not observed in phase VI and thus not considered here.) This point symmetry operation creates from a reciprocal cell of the derived phase (corresponding to one domain) a differently oriented reciprocal cell (corresponding to another domain). This procedure has to be applied to each of the four domains of the parent structure (phase IV). Three cases have to be considered according to the three subgroups of  $2/m$ . Two cases with a monoclinic reciprocal cell (for the subgroups 2 and  $m$ ) and one case with a triclinic reciprocal cell (for the subgroup  $\bar{1}$ ). The actual subgroup has to be compatible with the observed diffraction pattern.

The procedure is all performed in reciprocal space and consists of the following steps.

- (1) We start with the  $bc$  cell of phase II and choose the coordinate axes of reciprocal space  $x^*$ ,  $y^*$  and  $z^*$  to be parallel to  $[100]$ ,  $[010]$  and  $[001]$ , respectively.
- (2) The mirror plane of phase IV is then parallel either to the  $y^*z^*$ -plane or to the  $x^*z^*$ -plane. For the sake of the argument we consider the first possibility. The twofold axis is then parallel to  $x^*$ . Phase IV consists of 4 domains which transform into each other by a rotation of  $90^\circ$  about the  $z^*$ -axis [19].
- (3) For every one of the 4 domains in phase IV, one chooses a *monoclinic* reciprocal cell of the derived phase if the supposed symmetry is 2 or  $m$  or a *triclinic* one if it is  $\bar{1}$ . The axes of this cell are designated by  $a^*$ ,  $b^*$  and  $c^*$ . The origin of these reciprocal cells coincides with the origin of reciprocal space. The  $c^*$ -axes coincide with the  $z^*$ -axis of the chosen reciprocal space coordinate frame.
- (4a) Let the point symmetry of phase VI be  $m$ . The symmetry element lost on the transition is 2 and consequently every one of the 4 monoclinic reciprocal cells has to be rotated about the two-fold axis in order to generate a twin. By this procedure 8 monoclinic reciprocal cells are created with different orientations.
- (4b) Let the point symmetry of phase VI be 2. The symmetry element lost on the transition is  $m$  and consequently (the same) 8 monoclinic reciprocal cells are created as in (4a).
- (4c) Let the point symmetry of phase VI be  $\bar{1}$ . The symmetry elements lost on the transition are 2 and  $m$ . Consequently each of the 4 triclinic reciprocal cells has to be rotated about the twofold axis and to be reflected at the mirror plane (perpendicular to the twofold axis). The number of generated reciprocal cells is also 8 (and not 16) because a twofold axis and a perpendicular mirror plane imply the inversion center and vice versa.

Comparing the experimentally recorded splitting patterns with those following from the above procedures one is led to the conclusion that the actual cell must be tri-

clinic. A part of the reciprocal lattice that consists of 8 such triclinic cells is shown in Figure 8.

The three coordinates of a reflection in reciprocal space were determined by taking two coordinates from the Weissenberg photographs and the third from the corresponding rotating crystal photograph. The different types of possible splittings and the appearance of the corresponding Bragg reflections on a Weissenberg photograph are shown schematically in Figure 9.

One can describe the triclinic structure of phase VI as a distorted face centered NaCl cell. The corresponding dimensions are listed in Figure 4. From these values the reduced cell and its Niggli matrix representation were calculated [26]. It shows that the structure is truly triclinic. Therefore the observed extinctions (except those by the face centering) have to be considered as accidental (not implied by the space group but corresponding to the space group extinctions of phase IV).

Paramagnetic resonance indicates that the  $\text{O}_2^-$ -molecules in a domain are parallel to each other and to (100) or (010) planes of the triclinic *fc* cell shown in Figure 4. At 9 K the angle of tilt with respect to the triclinic *c*-axis (parallel to the [001]-axis of phase II) is  $29.5^\circ$  [20].

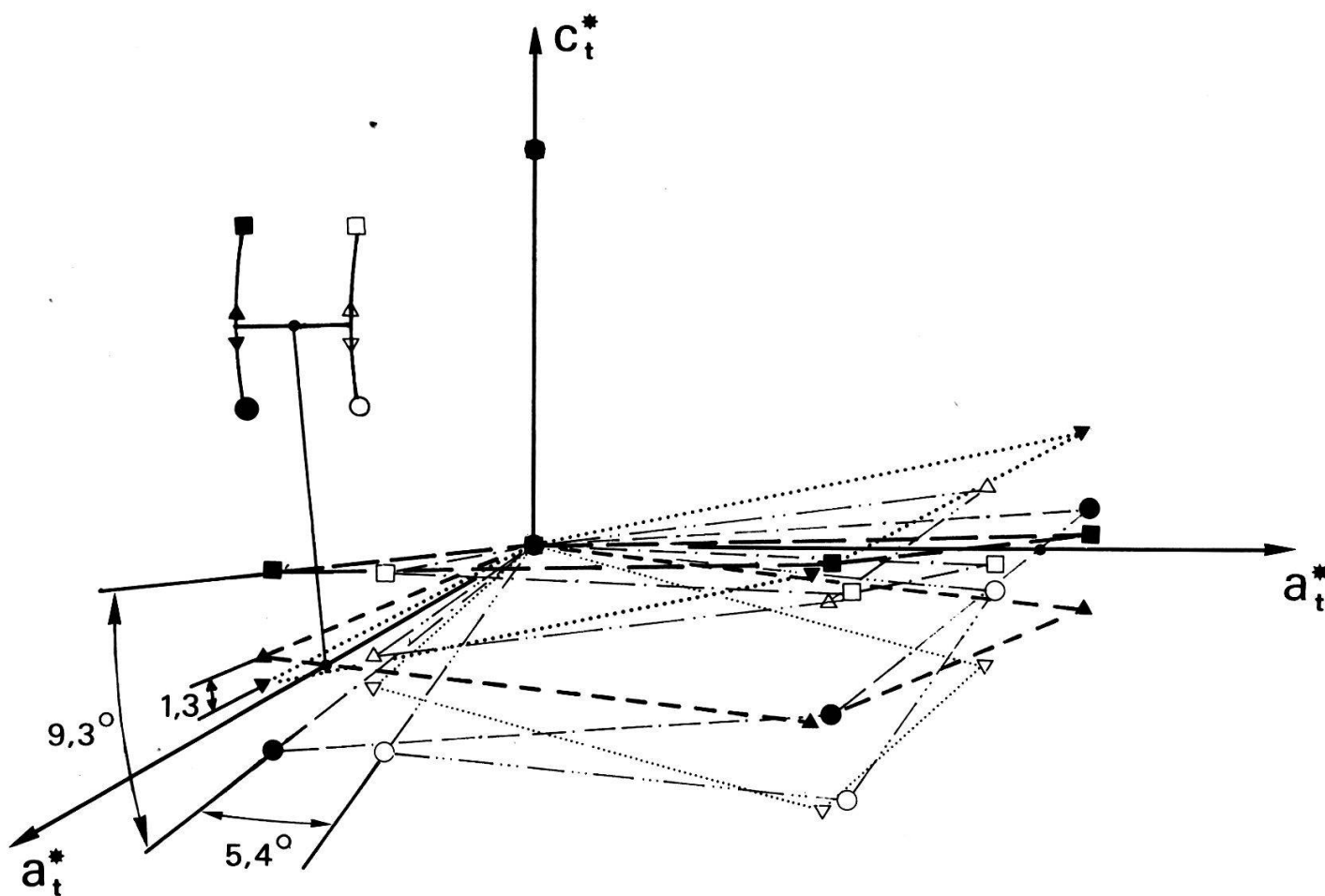


Figure 8

Part of the reciprocal lattice of a eight-domain  $\text{KO}_2$  crystal in phase VI. For sake of clarity only the reflections 100, 010, 110 and 001 (referred to the *bc* cell of phase II) are shown. Each domain is represented by a different geometrical symbol.

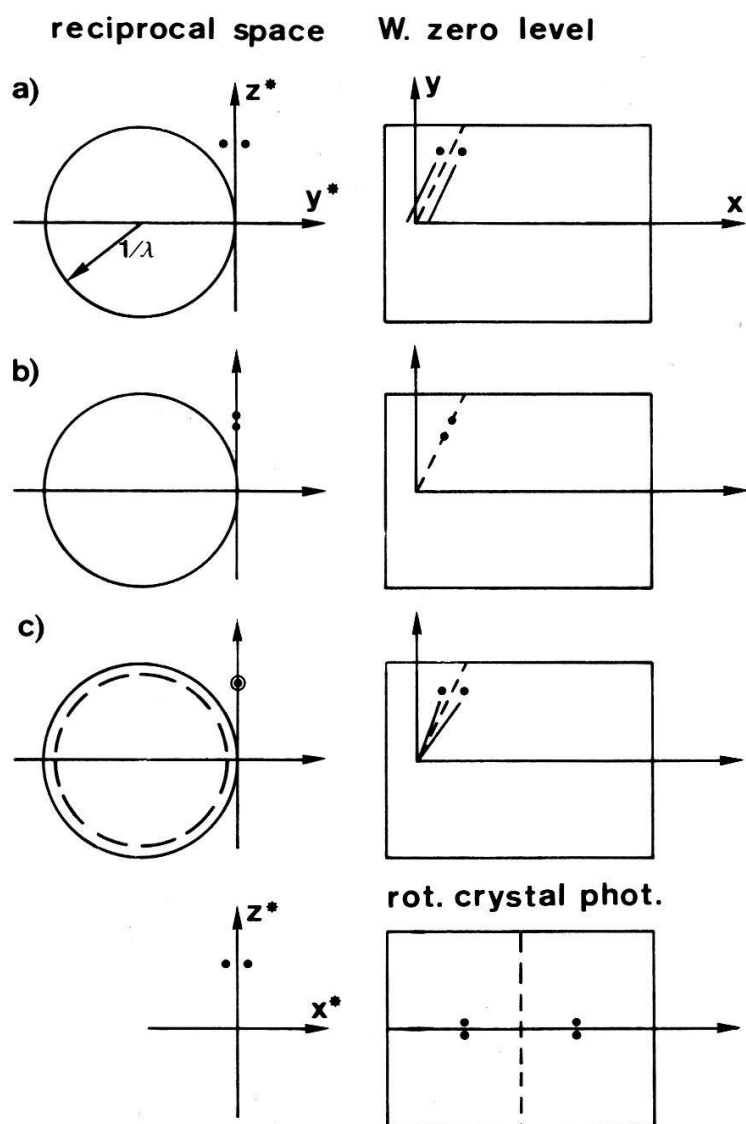


Figure 9

Schematic representation of the splitting of a central row in reciprocal space and the appearance of the reflections on Weissenberg zero level and rotating crystal photographs. The rotation axis of the crystal is parallel to the  $x^*$ -axis of the reciprocal space coordinate frame.

- (a) Splitting in the  $y^*z^*$ -plane.
- (b) Splitting in the  $y^*z^*$ -plane, along a central row.
- (c) Splitting in the  $x^*z^*$ -plane. The reflections will reach the film only if the slit between the layer line screens is wide enough. The reciprocal lattice points cut the Ewald sphere on the dashed circle.

**3.3.3. Actual crystallographic domain formation.** Group theory cannot predict the actual domain configuration in a real crystal. In addition to symmetry restrictions it depends upon boundary conditions, external and internal stresses, shape of the crystal, imperfections, thermal cycling etc. One can imagine a sequence of twinning processes that results in a larger number of domain orientations than predicted by simple group theory based on the equivalence of single twinning processes. In our experiments the following factors are certain to have a serious influence on the reproducibility of domain structure:

- (1) The mechanical stresses exerted upon the sample by the Lindemann capillary are not reproducible (the crystals are very soft) and, moreover, differ for the orientations (1) and (2) on the one hand and orientation (3) (described in Section 3.3.1) on the other.

- (2) In the temperature range of phase V two different structures coexist. Both of them are twinned. The volume fraction of the crystal that has the structure of phase IV diminishes with decreasing temperature.

The observed domain patterns differed from crystal to crystal, and some of them could not be interpreted on the basis of the simple group theoretical arguments presented in the previous section. However, two different crystals were found that (investigated in a different orientation) gave fully consistent twinning patterns. These were used for the analysis. The resulting cell dimensions can be considered correct with high probability.

A further experimental difficulty is the following. The X-ray reflections of crystals that have undergone several cooling cycles are unsharp because the crystals tend to shatter due to the large crystallographic distortions.

## 4. $\text{RbO}_2$

The structures of the low temperature phases known from previous and the present work are summarized in Figure 10. Again the pseudotetragonal  $bc$  cell of phase II is chosen as the reference system.

### 4.1. Sample mounting

The mounting is quite similar to that of the  $\text{KO}_2$ -crystals as described in Section 3.3.1. The same three orientations were used. The shape of the crystals differed from sample to sample, for most of them being a rectangular parallelepiped with truncated corners. The longest dimension of the crystals was usually parallel to  $[111]$ .

### 4.2. Crystallographic phase transitions

Rotating crystal photographs  $[001]$  and  $[110]$  axes parallel to the rotation axis are shown in Figures 11 and 12 as a function of the temperature. The Bragg angles of selected reflections are summarized in Table 1. As an illustration Weissenberg zero level photographs with rotation axis  $[001]$  taken at 100 K and 10 K are reproduced in Figure 13.

The interpretation of the X-ray diffraction patterns is that at low temperatures  $\text{RbO}_2$  does not behave like  $\text{KO}_2$ . The striking differences are the following:

- (1) The sharp incommensurate superstructure reflections (satellites) observed in phase III  $[2]$  persist upon cooling into phase V. Within experimental error there is no change of the modulation period  $(3.12 \pm 0.02)a$ .
- (2) Phase III can be subdivided into three subphases  $\alpha$ ,  $\beta$  and  $\gamma$  with the symmetries tetragonal, orthorhombic and monoclinic, respectively [27]. The temperature ranges where the transitions occur have not been investigated in detail (see Figure 10). The  $00l$  reflections do not split in the phases III to V (see Figure 12). Thus the  $[001]$ -axis is common to the phases III ( $\alpha$ ,  $\beta$ ,  $\gamma$ ) and V. In the monoclinic phases III $\gamma$  and V the  $[001]$ -axis becomes the twofold axis.

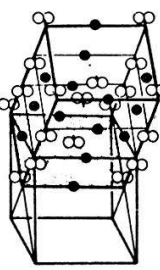
| RbO <sub>2</sub>                    |  |                          |  |  |
|-------------------------------------|--|--------------------------|--|--|
| Phase transition temp.              | Symmetry of unit cell of average structure | Symmetry of a domain     | State of order   | Lattice constant of average structure<br>Volume of unit cell   |
| II<br>[2, 15, 28, *]<br>194 K       | (as KO <sub>2</sub> II)                    | domains not investigated | (as KO <sub>2</sub> II)  | $a = 4.215 \pm 0.005 \text{ \AA}$<br>$c = 7.004 \pm 0.002 \text{ \AA}$<br>$V_{II} = 124.435 \text{ \AA}^3$   |
| III $\alpha$<br>[2, *]<br>135-175 K | bc-cell is pseudo-tetragonal               | orthorhombic             | <br>strongly correlated stacking, modulated structure, sharp incommensurate diffraction satellites, presumably due to antiphase domains, superperiod referred to bc-cell 3.12 a. | $a = 4.164 \pm 0.005 \text{ \AA}$<br>$c = 7.004 \pm 0.002 \text{ \AA}$<br>$V_{III\alpha} = 121.442 \text{ \AA}^3 = 0.976 V_{II}$   |
| III $\beta$<br>[*]<br>70-90 K       | bc-cell is orthorhombic                    | orthorhombic             |  | $a = 4.117 \pm 0.005 \text{ \AA}$<br>$b = 4.158 \pm 0.005 \text{ \AA}$<br>$c = 7.004 \pm 0.002 \text{ \AA}$<br>$V_{III\beta} = 119.898 \text{ \AA}^3 = 0.987 V_{III\alpha}$                                    |
| III $\gamma$<br>[*]<br>15.1 K       | bc-cell is monoclinic                      | monoclinic               |  | $a = 4.105 \pm 0.002 \text{ \AA}$<br>$b = 4.146 \pm 0.002 \text{ \AA}$<br>$c = 7.004 \pm 0.002 \text{ \AA}$<br>$\gamma = 90.69 \pm 0.01^\circ$<br>$V_{III\gamma} = 119.195 \text{ \AA}^3 = 0.994 V_{III\beta}$ |
| IV<br>[1]<br>14.7 K                 | was not investigated                       |                          |  |  |
| V<br>[30, *]                        | bc-cell is monoclinic                      | monoclinic               | (as III)<br>(presumably antiferromagnetic)   | $a = 4.099 \pm 0.002 \text{ \AA}$<br>$b = 4.148 \pm 0.002 \text{ \AA}$<br>$c = 7.003 \pm 0.002 \text{ \AA}$<br>$\gamma = 90.71 \pm 0.01^\circ$<br>$V_V = 119.060 \text{ \AA}^3 = 0.999 V_{III\gamma}$          |

Figure 10

Survey over the structures of the low temperature phases of RbO<sub>2</sub>. \* means reference to the present work. Average structure is here defined as the structure resulting from the regular Bragg reflections only [29]. In the monoclinic phases III $\gamma$  and V the first setting was chosen to emphasize the relation to the high temperature phases.



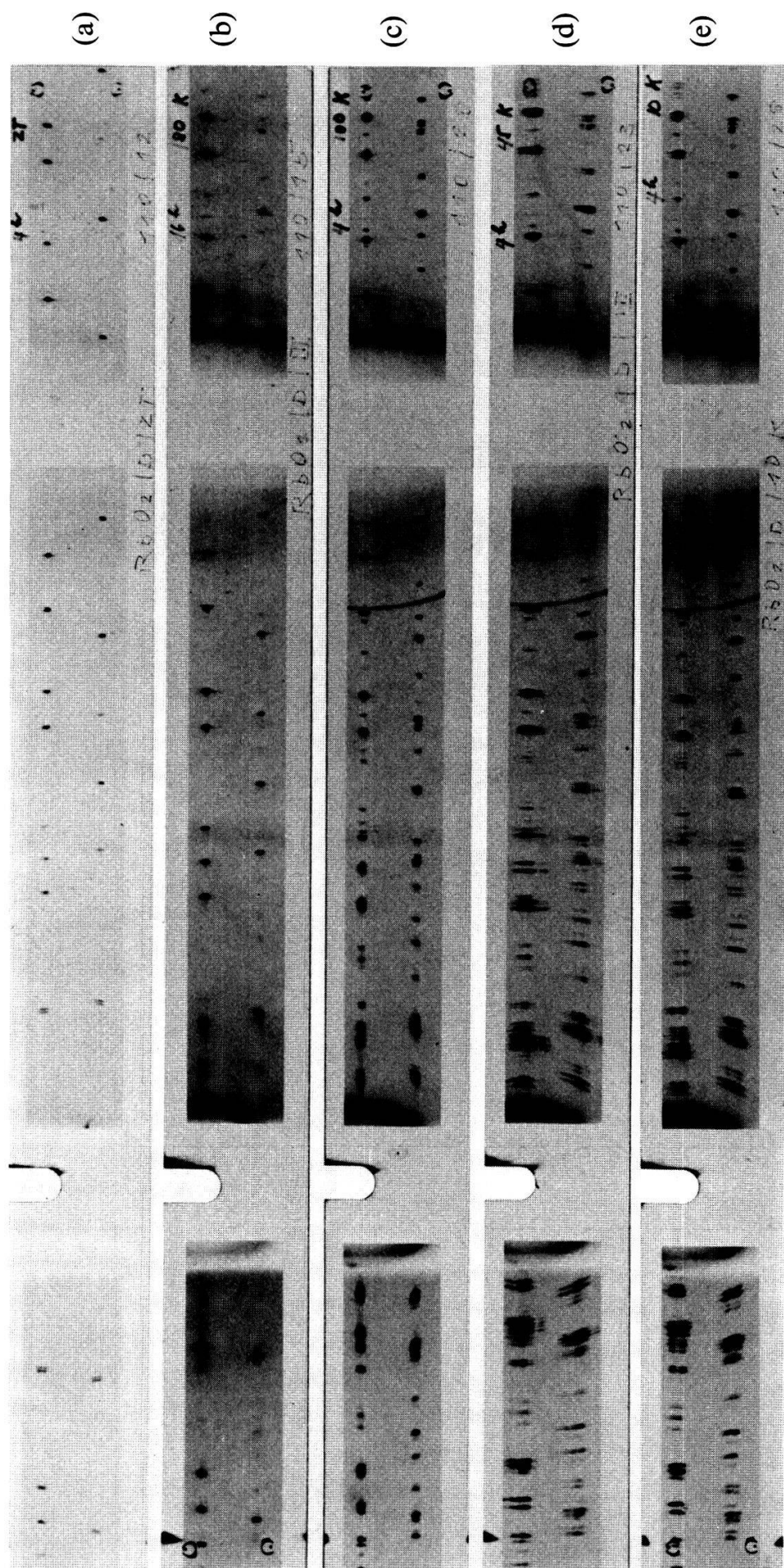


Figure 11

Rotating crystal photographs of  $\text{RbO}_2$  as function of temperature, crystal rotated about  $[001]$  (referred to phase II),  $\text{CuK}_\alpha$ -radiation (graphite monochromator), camera diameter 114.6 mm.

- (a) Phase II, 293 K, zero and first layer line.
- (b) Phase III $\alpha$ , 180 K, no splitting, weak satellite reflections appear in the zero and first layer line. Exposure time four times longer than in the photographs in (a), (c), (d) and (e).
- (c) Phase III $\beta$ , 100 K, primary splitting along the layer line, satellite reflections stronger than in (b).
- (d) Phase III $\gamma$ , 45 K, secondary splitting along the layer line and smearing out along Debye-Scherrer arcs.
- (e) Phase V, 10 K, as in (d).



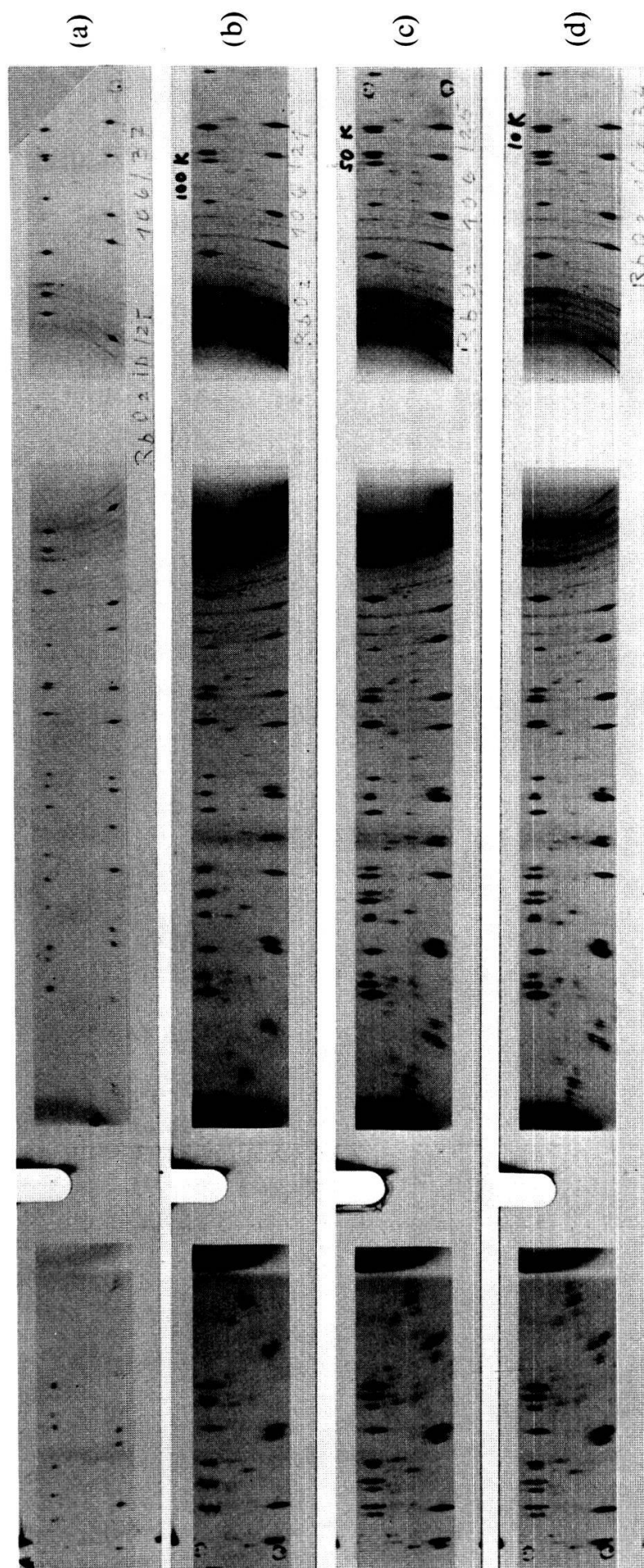


Figure 12

Rotating crystal photographs of  $\text{RbO}_2$  as function of temperature, crystal rotated about  $[110]$  (referred to the  $bc$  cell of phase II),  $\text{CuK}_\alpha$ -radiation (graphite monochromator), camera diameter 114.6 mm:

- (a) Phase II, 293 K, zero and first layer line.
- (b) Phase III $\beta$ , 100 K, layer lines of satellite reflections between the zero and first layer, no splitting.
- (c) Phase III $\gamma$ , 50 K, 00 $l$  reflections stay unsplit, the others split.
- (d) Phase V, 10 K, as in (c).

Table I  
Bragg angles of selected reflections of  $\text{RbO}_2$  as a function of temperature, indexed in reference to the  $bc$  cell. ( $\text{CuK}_{\alpha 1}$ -radiation).

| 180 K |     |     |                       | 100 K |     |     |                       | 45 K |     |     |                       | 10 K |     |     |                       |
|-------|-----|-----|-----------------------|-------|-----|-----|-----------------------|------|-----|-----|-----------------------|------|-----|-----|-----------------------|
| $h$   | $k$ | $l$ | Observed<br>two theta | $h$   | $k$ | $l$ | Observed<br>two theta | $h$  | $k$ | $l$ | Observed<br>two theta | $h$  | $k$ | $l$ | Observed<br>two theta |
| 1     | 1   | 0   | 30.440                | 1     | 1   | 0   | 30.640                | -1   | 1   | 0   | 30.503                | -1   | 1   | 0   | 30.520                |
|       |     |     |                       |       |     |     |                       | 1    | 1   | 0   | 30.907                | 1    | 1   | 0   | 30.945                |
| 2     | 2   | 0   | 63.230                | 2     | 2   | 0   | 63.790                | -2   | 2   | 0   | 63.374                | -2   | 2   | 0   | 63.390                |
|       |     |     |                       |       |     |     |                       | 2    | 2   | 0   | 64.234                | 2    | 2   | 0   | 64.334                |
| 3     | 1   | 0   | 71.735                | 1     | 3   | 0   | 71.998                | -1   | 3   | 0   | 71.842                | -1   | 3   | 0   | 71.810                |
|       |     |     |                       | 3     | 1   | 0   | 72.647                | 1    | 3   | 0   | 72.436                | 1    | 3   | 0   | 72.540                |
|       |     |     |                       |       |     |     |                       | 3    | 1   | 0   | 73.065                | 3    | 1   | 0   | 73.260                |
| 4     | 0   | 0   | 95.578                | 0     | 4   | 0   | 95.748                | 0    | 4   | 0   | 96.034                | 0    | 4   | 0   | 96.070                |
|       |     |     |                       | 4     | 0   | 0   | 96.944                | 4    | 0   | 0   | 97.266                | 4    | 0   | 0   | 97.560                |
| 3     | 3   | 0   | 103.253               | 3     | 3   | 0   | 104.350               | -3   | 3   | 0   | 103.807               | -3   | 3   | 0   | 103.900               |
|       |     |     |                       |       |     |     |                       | 3    | 3   | 0   | 105.578               | 3    | 3   | 0   | 105.690               |
| 4     | 2   | 0   | 111.680               | 2     | 4   | 0   | 112.268               | -2   | 4   | 0   | 111.857               | -2   | 4   | 0   | 111.900               |
|       |     |     |                       | 4     | 2   | 0   | 113.266               | 2    | 4   | 0   | 113.478               | 2    | 4   | 0   | 113.570               |
|       |     |     |                       |       |     |     |                       | 4    | 2   | 0   | 114.556               | 4    | 2   | 0   | 114.820               |
|       |     |     |                       |       |     |     |                       | -1   | 5   | 0   | 141.991               | -1   | 5   | 0   | 141.900               |
| 5     | 1   | 0   | 141.188               | 1     | 5   | 0   | 141.706               | 1    | 5   | 0   | 143.577               | 1    | 5   | 0   | 143.470               |
|       |     |     |                       | 5     | 1   | 0   | 144.874               | -5   | 1   | 0   | 145.219               | -5   | 1   | 0   | 145.690               |
|       |     |     |                       |       |     |     |                       | 5    | 1   | 0   | 146.927               | 5    | 1   | 0   | 147.530               |
| 0     | 0   | 2   | 25.420                | 0     | 0   | 2   | 25.518                | 0    | 0   | 2   | 25.499                | 0    | 0   | 2   | 25.486                |
| 0     | 0   | 4   | 52.195                | 0     | 0   | 4   | 52.232                | 0    | 0   | 4   | 52.252                | 0    | 0   | 4   | 52.222                |
| 0     | 0   | 6   | 82.576                | 0     | 0   | 6   | 82.579                | 0    | 0   | 6   | 82.599                | 0    | 0   | 6   | 82.587                |
| 0     | 0   | 8   | 123.230               | 0     | 0   | 8   | 123.219               | 0    | 0   | 8   | 123.223               | 0    | 0   | 8   | 123.267               |

According to caloric and magnetic measurements [1] phase IV exists in a temperature interval that is only 0.4 K wide. The temperature stability of the X-ray cryostat did not permit a study of this intermediate phase. At the transition  $\text{III}\gamma \rightarrow \text{V}$  no change in symmetry has been detected in X-ray diffraction. However, a small change of the unit cell dimensions occurs (see Figure 10).

Just below the transition  $\text{II} \rightarrow \text{III}$  the intensity of the satellite reflections is much lower than that of the Bragg reflections, it increases with decreasing temperature down to about 100 K and then levels off between 100 K to 10 K. It is known that the intensity of the satellite reflections is influenced by the parameters of the  $\text{O}_2^-$ -molecule [2]. One can conclude that they change significantly between 194 K and 100 K.

The changes of the reflection pattern due to symmetry lowering and the formation of differently oriented domains were analysed. The different orientations as such do not give rise to a splitting of the regular Bragg reflections on [001]-rotation photographs (Figure 11). In the phases  $\text{III}\alpha$  and  $\text{III}\beta$  the domains that correspond to a satellite formation in the [100]- and [010]-direction can be transformed into each

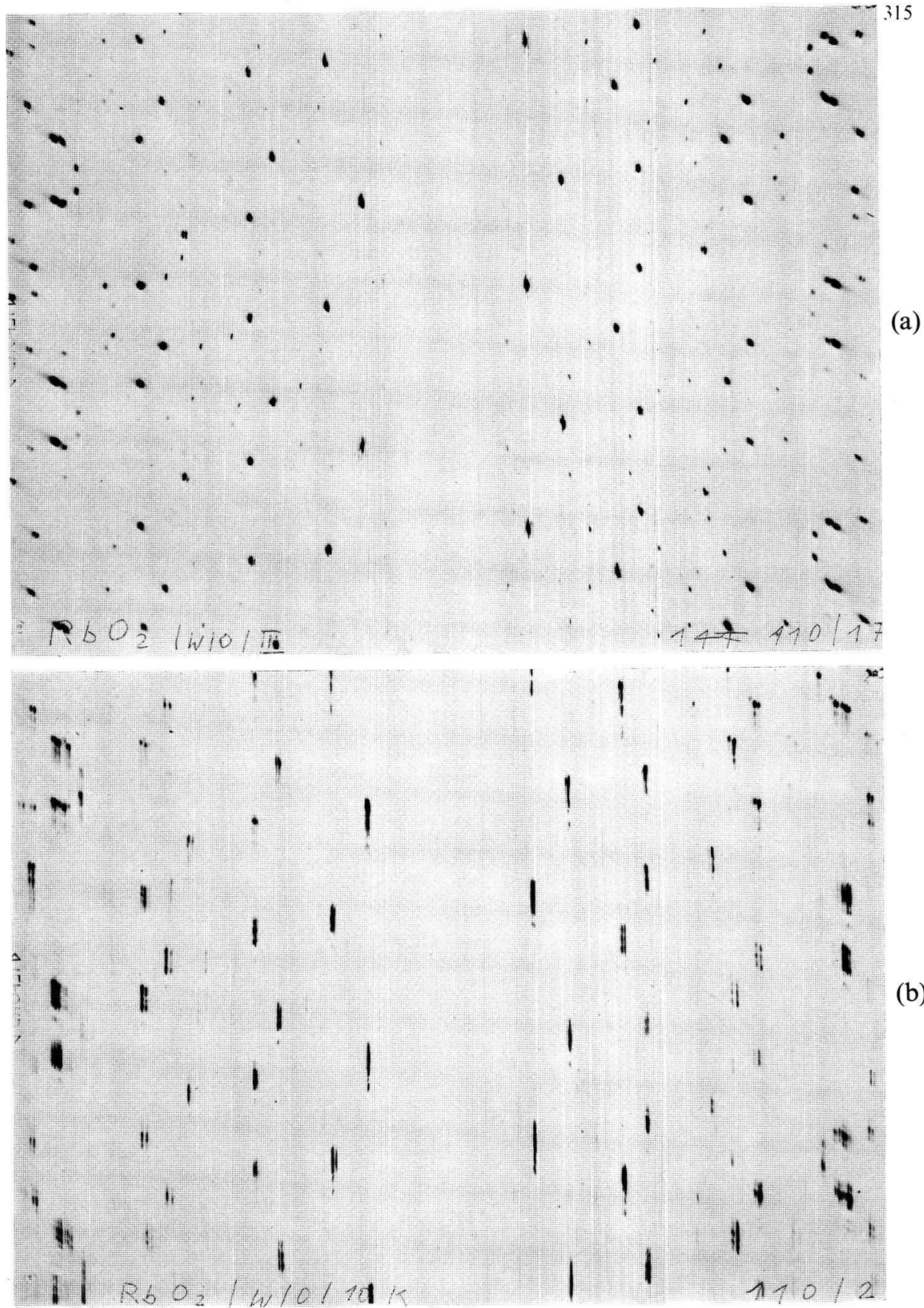


Figure 13

Weissenberg zero level photographs of RbO<sub>2</sub>, crystal rotated about [001] (referred to phase II), CuK $\alpha$ -radiation (graphite monochromator).

- (a) Phase III $\beta$ , 100 K, Bragg and satellite reflections, splitting observable in the backscattering region.
- (b) Phase V, 10 K, Bragg and satellite reflections, several reflections spread in a row due to angular spread of the orientation of the [001]-axis.



other by a  $90^\circ$ -rotation about  $[001]$ . The splitting of the regular Bragg reflections in Figure 11 (c) (phase  $\text{III}\beta$ ) is due to the lowered (orthorhombic) symmetry of the  $bc$  cell. In the (monoclinic) phases  $\text{III}\gamma$  and V the domains can be transformed for example by a  $180^\circ$ -rotation about  $[100]$  and  $[010]$ . The splitting of the Bragg reflections *along* the layer lines in figures 11 (d) and (e) is due to the monoclinic deformation of the  $bc$  cell. It is striking that the reflections are smeared out along sharp Debye–Scherrer arcs, this indicates an angular spread of the orientations of the domains. The extreme values of the spread depend upon the sample, for most samples it was about  $1.7^\circ$ . However, there was one crystal individual with a spread of  $9^\circ$ . Figure 13 (b) illustrates a spread of  $1.7^\circ$  in a Weissenberg photograph.

## 5. $\text{CsO}_2$

The structures of the low temperature phases known from previous and the present work are summarized in Figure 14. Again the tetragonal  $bc$  cell of phase II is chosen as the reference system. The mounting and the shape of the crystals are as described for  $\text{RbO}_2$  in Section 4.1.

Weissenberg zero level photographs at two different temperatures are shown in Figure 15 for rotation about  $[100]$ .

The interpretation of the diffraction patterns is that the structures of the low temperature phases of  $\text{CsO}_2$  differ from those of  $\text{KO}_2$  and  $\text{RbO}_2$ . In contrast to  $\text{KO}_2$  the sharp diffraction satellites observed in phase III [2] persist upon cooling into phase IV without change of the modulation period  $(3.45 \pm 0.02)a$ . The main difference from  $\text{RbO}_2$  is that the symmetry of the  $bc$  cell is orthorhombic throughout phases III and IV over the whole temperature range investigated (5–190 K). The  $00l$  reflections do not split.

The transition  $\text{II} \rightarrow \text{III}$  (at 190 K) is the only one at which twinning was observed. This twinning is analogous to that which would correspond to a transition  $\text{II} \rightarrow \text{III}\beta$  in  $\text{RbO}_2$ . An angular spread of the domain orientation as observed in  $\text{RbO}_2$   $\text{III}\gamma$  and V does not occur. Apparently in  $\text{RbO}_2$  this spread is due to the monoclinic deformation. However, small changes in the dimensions of the unit cell occur as is summarized in Figure 14.

Two crystals were found that showed a different behaviour than described above. In one crystal, the symmetry of the  $bc$  cell remained tetragonal through phases III and IV, although the satellite reflections appeared. In the other crystal, the phase transition  $\text{II} \rightarrow \text{III}$  did not manifest itself at all [31].  $\text{CsO}_2$  is even more sensitive to internal and external stresses than  $\text{KO}_2$  and  $\text{RbO}_2$ .

## 6. Discussion

At high temperatures (phases I, II and III) there is a very close relationship between the structures of the different alkali hyperoxides with the exception of  $\text{NaO}_2$ . However, at low temperatures each compound develops its individuality. X-ray diffraction revealed phases that were not distinguishable by magnetic and caloric measurements and vice versa.

The transition  $\text{IV}/(\text{V})/\text{VI}$  in  $\text{KO}_2$  is accompanied by a large distortion of the lattice and, according to paramagnetic resonance [20], a reorientation of the  $\text{O}_2^-$ -molecules. X-ray crystallography qualifies phase V as a coexistence of the structures

| CsO <sub>2</sub>         |  |                          |   |   |       |
|--------------------------|--|--------------------------|---|---|-------|
| Phase transition temp.   | Symmetry of unit cell of average structure | Symmetry of a domain     | State of order                                    | Lattice constant of average structure<br>Volume of unit cell  |       |
| II<br>[2,15,28]<br>190 K | (as KO <sub>2</sub> II)                    | domains not investigated | (as KO <sub>2</sub> II)                           | $a = 4.477 \text{ \AA}$<br>$c = 7.350 \text{ \AA}$<br>$V_{II} = 147.320 \text{ \AA}^3$  | 293 K |
| III                      | bc-cell is orthorhombic                    | orthorhombic             | (as KO <sub>2</sub> III,<br>RbO <sub>2</sub> III) | $a = 4.552 \pm 0.01 \text{ \AA}$<br>$b = 4.402 \pm 0.02 \text{ \AA}$<br>$c = 7.334 \pm 0.005 \text{ \AA}$<br>$V_{III} = 146.958 \text{ \AA}^3 = 0.998 V_{II}$ | 160 K |
|                          |  |                          |   | $a = 4.457 \pm 0.01 \text{ \AA}$<br>$b = 4.37 \pm 0.02 \text{ \AA}$<br>$c = 7.336 \pm 0.005 \text{ \AA}$<br>$V_{III} = 142.884 \text{ \AA}^3 = 0.970 V_{II}$  | 100 K |
|                          |  |                          |   | $a = 4.461 \pm 0.01 \text{ \AA}$<br>$b = 4.38 \pm 0.02 \text{ \AA}$<br>$c = 7.337 \pm 0.005 \text{ \AA}$<br>$V_{III} = 143.686 \text{ \AA}^3 = 0.975 V_{II}$  | 85 K  |
| [2,*]<br>9.6 K           | bc-cell is orthorhombic                    | orthorhombic             | (as III)<br>(presumably antiferromagnetic)        | $a = 4.460 \pm 0.01 \text{ \AA}$<br>$b = 4.375 \pm 0.05 \text{ \AA}$<br>$c = 7.336 \pm 0.005 \text{ \AA}$<br>$V_{IV} = 143.144 \text{ \AA}^3 = 0.972 V_{II}$  | 8 K   |
| IV<br>[2,30,*]           |  |                          |   |   |       |

Figure 14

Survey over the structures of the low temperature phases of CsO<sub>2</sub>. For explanation see the caption of Figure 10.

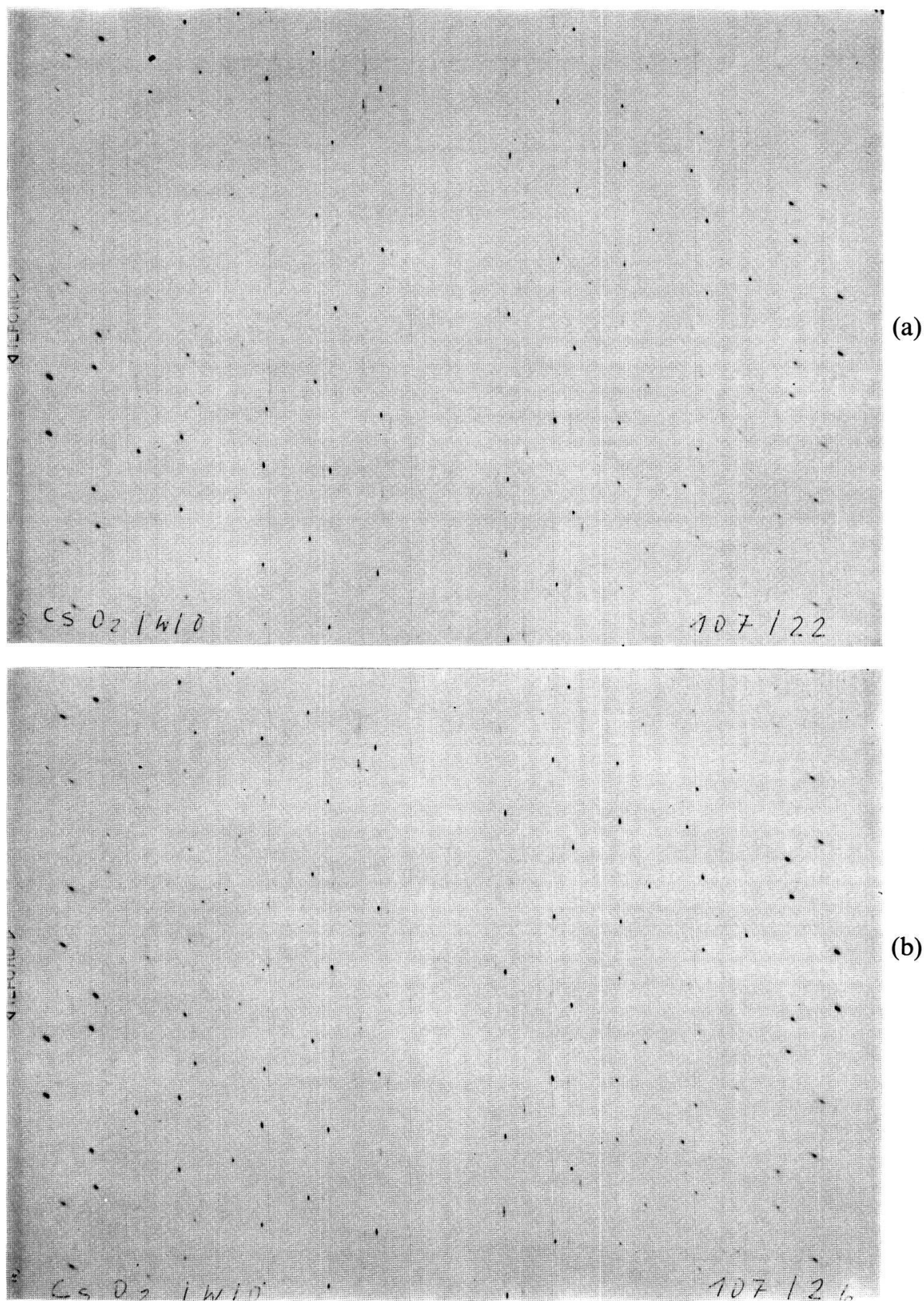


Figure 15  
Weissenberg zero level photographs of  $\text{CsO}_2$ , crystal rotated about  $[100]$  (referred to the  $bc$  cell of phase II),  $\text{CuK}_\alpha$ -radiation (graphite monochromator): (a) phase III, 85 K, (b) phase IV, 8 K.



of phases IV and VI. *Paramagnetic resonance* indicates the onset of a short-range magnetic order between 7 and 12 K [1, 20]. It seems that at low temperatures the coupling between molecular and magnetic order gives rise to very complicated partially ordered phases that may only be metastable.  $\text{KO}_2$  is not the only crystalline solid exhibiting the coexistence of two structures in a finite temperature interval. Other examples are the coexistence of austenite and martensite in steel [32], and KCN where even a new structure can be induced by a certain composite temperature cycle [33–36].

In  $\text{RbO}_2$  and  $\text{CsO}_2$  the modulated structure which in  $\text{KO}_2$  is observed in phase III persists down to 5 K. This implies at best molecular short-range order whereas in  $\text{KO}_2$  long-range molecular order below 196 K is not inconsistent with X-ray diffraction data [19]. The magnetic behaviour of  $\text{RbO}_2$  and  $\text{CsO}_2$  [1, 30] suggests antiferromagnetic order in the lowest temperature phase as for  $\text{KO}_2$ . The structure of phase IV of  $\text{KO}_2$  suggested that long-range parallel molecular order might be a prerequisite for the onset of long-range magnetic order.  $\text{RbO}_2$  and  $\text{CsO}_2$  seem to refute such a hypothesis.

## Acknowledgments

The authors wish to thank Dr. V. Janovec, M. Labhart, Dr. M. Bösch, P. Steiner, B. von Allmen, M. Rossinelli and Dr. H. Burkard for many discussions and experimental help. The technical assistance by H. R. Aeschbach and M. Wächter is gratefully acknowledged.

## REFERENCES

- [1] A. ZUMSTEG, M. ZIEGLER, W. KÄNZIG and M. BÖSCH, *Phys. cond. Matter* 17, 267 (1974).
- [2] M. ZIEGLER, M. ROSENFELD, W. KÄNZIG and P. FISCHER, *Helv. Phys. Acta* 49, 57 (1976).
- [3] M. ZIEGLER, J. SCHWEIZER, P. FISCHER and H. G. SMITH, Progress Report ILL, Grenoble (experiment number 05-04-021), 1976.
- [4] P. BRÜESCH, M. BÖSCH, W. KÄNZIG, M. ZIEGLER and W. BÜHRER, *Phys. stat. sol. (b)* 77, 153 (1976).
- [5] H. G. SMITH, R. M. NICKLOW, L. J. R. RAUBENHEIMER and M. K. WILKINSON, *J. Appl. Phys.* 37, 1047 (1966).
- [6] W. KÄNZIG and M. LABHART, *J. de Phys.* 37, C7–39 (1976).
- [7] M. BÖSCH and W. KÄNZIG, *Helv. Phys. Acta* 48, 743 (1975).
- [8] M. ZIEGLER, M. BÖSCH and H. AREND, Presented at the First European conference on crystal growth, Zürich, September 12–18, 1976, p. 200.
- [9] G. KLIPPING, *Kältetechnik* 13, 250 (1961).
- [10] G. HÖHNE, G. KLIPPING, J. LUDEWIG, A. TIPPE and H. WALTER, *Z. angew. Phys.* 25, 250 (1968).
- [11] G. KLIPPING, D. VETTERKIND and G. VALENTOWITZ, *Cryogenics* 5, 76 (1965).
- [12] ROBERT HUBER, *Diffractionstechnik*, 8211 Rimsting (West Germany).
- [13] Stoe + Cie GmbH, 61 Darmstadt, West Germany.
- [14] M. J. BUEGER, *X-ray crystallography* (J. Wiley & Sons 1942), chapter 14.
- [15] W. KASSATOCHKIN and W. KOTOW, *J. Chem. Phys.* 4, 458 (1936).
- [16] A. HELMS and W. KLEMM, *Z. anorg. allg. Chem.* 241, 97 (1939).
- [17] S. C. ABRAHAMS and J. KALNAJS, *Acta Cryst.* 8, 503 (1955).
- [18] F. HALVERSON, *J. Phys. Chem. Solids* 23, 207 (1962).
- [19] A. DE KOZAK, J. C. BARDIN and A. ERB, *Rev. Chimie min.* 13, 190 (1976).
- [20] M. ZIEGLER, H. R. MEISTER and W. KÄNZIG, *Helv. Phys. Acta* 48, 599 (1975).
- [21] M. LABHART, D. RAUX and W. KÄNZIG, *Helv. Phys. Acta* 50, 602 (1977).
- [22] V. JANOVEC, *Czech J. Phys.* B22, 974 (1972).

- [22] V. JANOVEC, V. DVOŘÁK and J. PETZELT, Czech J. Phys. *B25*, 1362 (1975).
- [23] G. VAN TENDELOO and S. AMELINCKX, Acta Cryst. *A30*, 431 (1974).
- [24] H. WONDRAATSCHEK and W. JEITSCHKO, Acta Cryst. *A32*, 664 (1976).
- [25] V. JANOVEC, Ferroelectrics *12*, 43 (1976).
- [26] L. V. AZÁROFF and M. J. BUEGER, *The Powder Method in X-ray Crystallography* (1958), chapter 11.
- [27] M. ACKERMANN, Diplomarbeit ETH, unpublished.
- [28] V. YA. DUDAREV, A. G. TSENTSIPER and M. S. DOBROLYUBOVA, Sov. Phys. Cryst. *18*, 477 (1974).
- [29] H. BÖHM, Acta Cryst. *A31*, 622 (1975).
- [30] M. LABHART, private communication.
- [31] N. MEDICI, Diplomarbeit ETH, unpublished.
- [32] J. W. CHRISTIAN, *The Theory of Transformations in Metals and Alloys* (1965), chapters 21 and 22.
- [33] A. CIMINO, G. S. PARRY and A. R. UBBELOHDE, Proc. Roy. Soc. *A252*, 445 (1959).
- [34] G. S. PARRY, Acta Cryst. *15*, 596 (1962).
- [35] G. S. PARRY, Acta Cryst. *15*, 601 (1962).
- [36] A. CIMINO and G. S. PARRY, Il Nuovo Cimento *19*, 971 (1961).